Integration of the components in a small-scale stationary research PEFC system

Cecilia Wallmark [a], Sofia Enbäck [b], Markku Rissanen [c],
Per Alvfors [a,*], Göran Lindbergh [b]

[a] *KTH – Royal Institute of Technology, Chemical Engineering and Technology, Energy Processes,
SE-100 44 Stockholm, Sweden*
[b] *KTH – Royal Institute of Technology, Chemical Engineering and Technology, Applied Electrochemistry,
SE-100 44 Stockholm, Sweden*
[c] *ABB AB, Corporate Research, SE-721 78 Västerås, Sweden*

Abstract

With the primary aim of studying the integration of the components in a polymer electrolyte fuel cell (PEFC) system, a test facility for research on small-scale stationary PEFC systems has been built at the Royal Institute of Technology in Stockholm. In this paper the PEFC system with control system and measurement equipment is described in detail together with the first experimental data. The research PEFC system has a flexible configuration and allows fuel cell systems from approximately 0.2 to 4 kW$_{el}$ to be tested. The main feed is natural gas, but the fuel cell stack can also be run on humidified hydrogen. The main limitation in the system integration is the power mismatch of the fuel cell stack and fuel processor. The paper begins with a literature review of research/test PEFC systems.
© 2005 Elsevier B.V. All rights reserved.

Keywords: Fuel cell system; Integration; Control system; Natural gas and hydrogen; Experiments; Start-up behaviour

1. Introduction

At present (2004), the first results from existing installations of series (>10 units) of residential polymer electrolyte fuel cell (PEFC) systems are published [1], and totally close to 2000 units of sizes 0.5–10 kW$_{el}$ have been built (e.g. [2,3]). Important results presented from demonstration units are the conclusions regarding system improvements. The suggested improvements often concern water handling, component sizing, start-up behaviour or heat transfer [13,14,7], but also treat real commercial issues such as water quality [15] and shipping and packaging [16]. Furthermore, the automatic control systems for some fuel cell pilot plants have been disclosed in the literature [17,18,11]. Several fuel cell companies and users have presented their fuel cell system properties and layouts [4–8], but have rarely described how the design solutions were found.

Additionally, also less central components, such as measuring equipment and, for example, safety valves are given for a few pure hydrogen test bench configurations [9–11], and for a pure hydrogen system [12].

Test benches for the development and research of pure hydrogen fuel cell systems have been described in the literature, e.g. in the range 0.5–1 kW$_{el}$ [19,20,9]. Results concerning the importance of humidification levels of the inlet flows, dynamics in combination with load [21–23] and control strategies [24] have been published. During the last few years the number of manufacturers offering test stands for fuel cell stacks has increased, and some have now enlarged the product spectrum to include test equipment for the reforming part of the system as well. Further, test systems including both fuel processing and a fuel cell stack may be found at universities and research institutes [25,26].

Various simulation studies of natural gas-fuelled PEFC systems have been performed during the last years. For example, researchers have presented the dependency of system efficiencies on the system pressure, compressor efficiencies [27], and

---

* Corresponding author. Tel.: +46 8 790 6526; fax: +46 8 723 0858.
E-mail address: alvfors@kth.se (P. Alvfors).

Nomenclature

ATR	combinatoral reformer (autothermal reformer)
CPO	catalytic partial oxidation
LTS	low temperature water–gas shift
NG	natural gas
O/F	oxygen-to-fuel ratio, definition mol O mol^{-1} fuel
PROX	preferential oxidation
S/C	steam-to-carbon ratio, definition mol H_2O mol^{-1} C in fuel
SR	steam reforming
WGS	water–gas shift

the reformer type [28]. Regarding systems including fuel processing, a simulation study [29] has recently been published displaying the water balance for different fuels in PEFC systems, including dependencies on fuel processor parameters, steam-to-carbon ratio (S/C), oxygen-to-fuel ratio (O/F), fuel utilisation, exhaust gas temperature and pressure, and fuel composition. Parameter variations in experiments with natural gas reformers have also been presented in the literature, [30], even in direct comparison with modelled data [31]. Important factors such as start-up times and strategies have also been studied [32] and dynamics, reactor design and control parameters have been discussed [33]. Research and development efforts concerning small fuel processors for hydrogen production are listed in a report by Ogden [34].

However, details and real problems with the design and the components in a research reformate-based system including complete measurement equipment have not yet been fully reported. The characteristics and interaction of all the components in a fuel cell system are as important as the function of
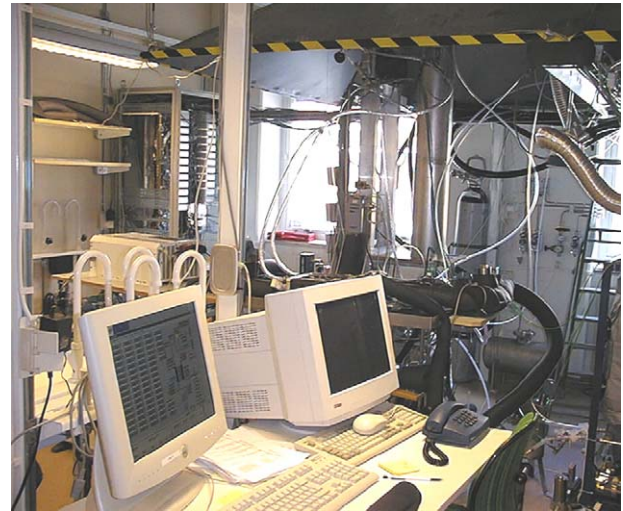

Fig. 1. The research laboratory. The components in the pilot plant are well spread-out in the room: the fuel cell stack on a table in the middle of the figure, the inverter and the control system rack to the left, and the fuel processor and the gas analysis to the right outside the picture.

the fuel cell stack and the fuel processor for the performance and total cost. Hence, the aim of this paper is to describe the integration of the components in a polymer electrolyte fuel cell system. However, a limitation of the system presented in this paper is that the fuel cell system described should not be considered optimal due to the poor availability of components and cost reasons at the time of purchase.

2. Description of the PEFC system

The research PEFC system (Fig. 1) has a flexible configuration and allows fuel cell systems from approximately 0.2 to
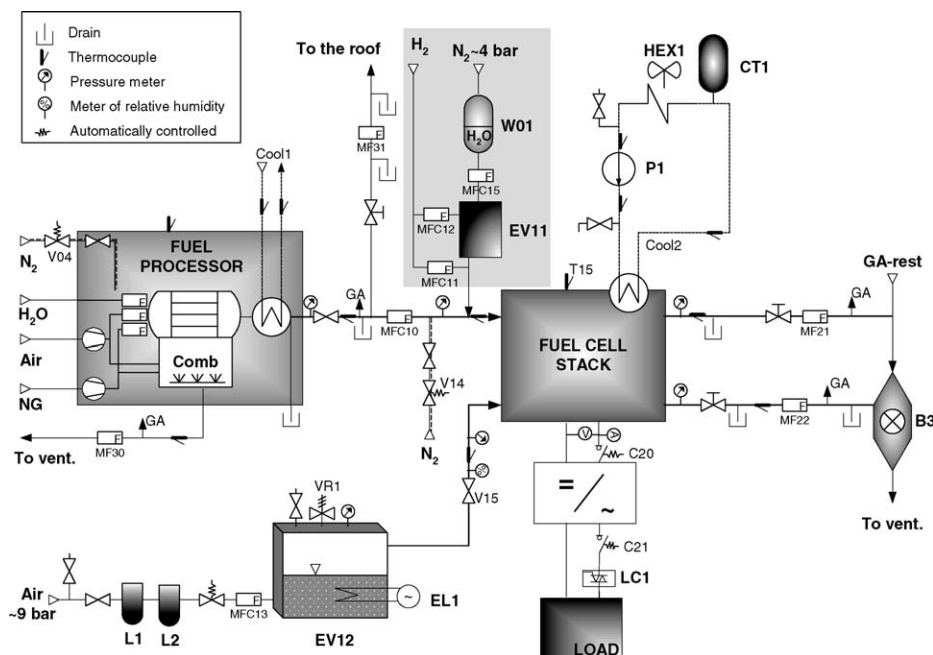

Fig. 2. A schematic view of the fuel cell system, see Appendix A for the list of symbols and detailed information on the components.

$4 \, kW_{el}$ in size to be tested. The main components are the fuel processor, the fuel cell stack, and the inverter together with the load. It is also equipped with a state-of-the-art gas analysis and control system. Numerous temperature, flow and pressure measurements are made in the system allowing analysis of mass and energy balances as well as system properties. The feed is either humidified hydrogen or natural gas, which is reformed to a hydrogen-rich gas (the reformate) in a fuel processor. The system components can be seen in the process diagram in Fig. 2 and their details are listed in Appendix A.

2.1. The fuel processor

The fuel processor is designed to provide reformate corresponding to an approximate range of $1–10 \, kW_{el}$. However, the control parameters have been adjusted by the manufacturer to better fit our purposes. That is, parameters that are more suited for $2–4 \, kW_{el}$. The product gas should contain approximately 50% hydrogen on a dry basis and less than 10 ppm CO and 2% methan (CH_4) according to the manufacturer.

The fuel processor has three main reactors, a combinatorial reforming reactor (ATR), a low temperature shift reactor (LTS) and a preferential oxidation reactor (PROX), see Fig. 3. The ATR includes both catalytic partial oxidation (CPO) and steam reforming (SR). The water fed to the ATR is pre-heated to steam. To increase the hydrogen production the steam reforming is heated by a combustor as well, this heat is furthermore important at the start-up of the fuel processor. The steam-to-carbon ratio and the oxygen-to-fuel ratio are variable inputs. Desulphurisation is included before the LTS, and the deliverer guarantees a sulphur level <500 ppb. The final CO clean-up is performed in a PROX reactor. The four steps in the PROX, separated by heat exchangers (HEX), are separately fed with successively decreasing air flows. The internal heat exchangers preheat the flows, produce steam for the steam reforming, and cool the reaction flows. The main heat exchanger cools the combustor exhaust.
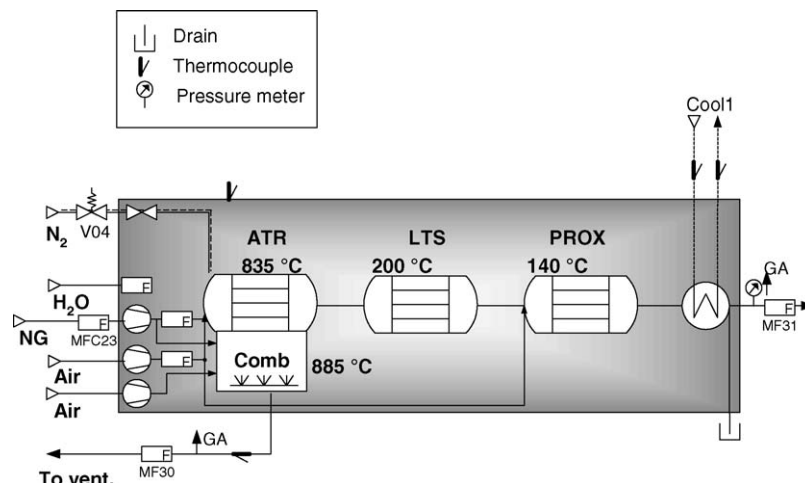
2.2. The fuel cell stack

The polymer electrolyte fuel cell stack initially used is designed for a maximum of $2 \, kW_{el}$ continuously. The stack has 68 cells, each about $120 \, cm^2$. The fuel cell stack is designed for reformate, but can be run on hydrogen as well. The stack is cooled by a fluorinated liquid that boils at $60 \, °C$. The fluid usually circulates by natural convection and releases heat to the surroundings through a heat exchanger before it flows down below the stack, where a pump is situated. In case of large loads, natural convection is not fast enough for the stack to be kept at $60 \, °C$, then the pump can speed up the flow rate of the cooling medium. At really high loads, there is a fan that cools the heat exchanger. The heat is not used within the system in the initial design.

2.3. The inverter and load system

To imitate a fuel cell system built to provide a building with alternating current an inverter is installed in the system. The load is an ordinary electrical radiator with pure resistive characteristics, whose power level is controlled by a signal from the control system. The load signal controls the power-regulating module LC1 in Fig. 2, which is based on an integral 26 A triac and uses variable phase angle control. The inverter is installed without connection to the power grid.

2.4. The water supply systems

There are three different water streams entering the system.

- The fuel processor is fed with de-ionised water at 3 bar(g) from the in-house system.
- For the anode, a mass flow controller delivers milli-Q water, W01, to a controlled evaporator mixer, EV11, which humidifies the hydrogen when running on pure hydrogen.
- The cathode air is humidified by passing through a tank, EV12, filled with milli-Q water. The temperature of the water

Fig. 3. The fuel processor includes three main reactors, ATR (combinatoral reforming), LTS (low temperature water–gas shift) and PROX (preferential oxidation), a combustor and heat exchangers. Typical inlet and reaction temperature levels are displayed in the figure.

in the tank is controlled, and a distributor at the bottom of the tank forces the air through the heated water.

2.5. The gas analysis system

Sample gas can be sucked from four points in the fuel cell system. The gas is sucked through heated sample lines via humidity sensors to the gas analysis system. When approximately $60 \, l \, gas \, h^{-1}$ is sucked per sample point, each point can be analysed within 120 s. The gas analysis system measures hydrogen, carbon dioxide, carbon monoxide, methane and oxygen. The system consists of three analyser modules and a gas sample cooler. Hydrogen is measured by a thermal conductivity analyser module. Carbon dioxide, carbon monoxide and methane are measured by an infrared analyser module. Furthermore, oxygen is measured in a magnet mechanical oxygen analyser module. The methane analyses include also higher hydrocarbons present, i.e. it is not possible to distinguish the content of higher hydrocarbons from the methane in the reformate gas. The gas streams are dried before they enter the analyser modules.

2.6. The fuel cell system integration

2.6.1. Main issues

To maintain the temperatures of the flue gases, which in this system flow long distances from one component to another, heating cables are mounted outside the pipes. Further, the housings of the humidity sensors are heated.

In this first set-up, the fuel processor is designed for larger load levels than the stack. The reason is that the number of components available for sale was strictly limited at the time, at the end of 2000. This has resulted in special solutions for the reformate feed and the exhaust streams. Only a limited part of the reformate flow is fed to the fuel cell stack with the help of a mass flow controller. To simplify the system configuration and to avoid problems with too low hydrogen content in the combustor, the anode exit gas is not fed back to the combustor, which would have been the case in a commercial system. A catalytic burner, B3, was installed to burn the excess hydrogen from the anode with the excess air from the cathode. The excess reformate is piped out through the wall and up above the roof. Further, the fuel processor tolerates a maximum back pressure of 0.35 bar(g) and the stack is designed to have a back pressure of 0.8 bar(g). The system was designed for a low operating pressure, which implies that the operation pressure even when running on pure hydrogen is limited.

2.6.2. The control system

The control system has three main tasks, namely surveying and controlling the system and logging data. It was delivered by ABB Utilities; Freelance 2000 is used as software. The system is based on the Industrial IT process station Advant Controller 800F for controlling and surveying of the system. The I/O modules are of type S800. The operator interface is built in DigiVis and the data logging is enlarged with the help of a so-called Trend server. The software DigiBrowse is used for viewing of
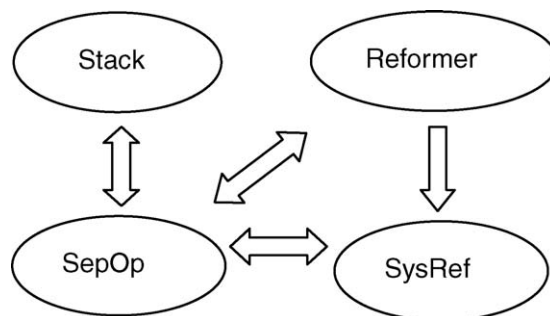

Fig. 4. The four different modes of running the fuel cell system and the possible transitions between them. The mode SepOp represents separate but simultaneous operation of the stack and the fuel processor, and SysRef when the stack is run on simultaneously produced reformate.

saved data. Totally 252 variables can be logged. This includes both signals and calculated values.

To maximise the usefulness of the test facility it can be run in four different modes, namely: the fuel processor alone, the stack alone, the fuel processor and the stack at the same time but separately, or as a system where the fuel cell stack is run on gas produced by the fuel processor. The different modes and the possible transitions between them can be seen in Fig. 4.

In order to control the switch between these modes the control system programming was divided into seven sequences, with the pilot sequence being master. Each sequence is built-up by states representing events and the corresponding surveillance functions based on IEC programming methodology [35]. To move from one step to another pre-decided conditions must be fulfilled. The complete description of the sequences, states, transitions and conditions is to be found in a separate specification.

The 'Reformer ON' button in the graphical user interface (GUI), Fig. 5, starts the fuel processor sequence, which controls the valves and regulators for the fuel processor. The stack sequence is divided into two parallel tracks where 'Stack Reformate ON' controls the valves and regulators, which are involved when running on reformate, and 'Stack H2 ON' controls the valves and regulators involved when running on humidified hydrogen. Either of the two buttons start the stack sequence, and depending on which button was pressed the sequence follows the corresponding track. The stack sequence starts the load sequence automatically. If the fuel processor has not already been started when the 'Stack Reformate ON' button is pressed, the fuel processor sequence is started automatically. A load profile can be programmed which makes it possible to have the same warming-up procedure each time the stack is started.

The remaining sequences are the gas analysis, the cooling and the auxiliary sequence. The auxiliary sequence is for the moment only used for surveying the catalytic burner. With the split of the fuel processor and the stack sequences, there is no risk of giving counter-orders to the mass flow regulators or to the valves, and there is no risk of trying to feed the stack with both hydrogen and reformate.

When starting the fuel cell system a nitrogen purge is performed. After initiation of the other sequences, the pilot goes into run mode. At this point any running mode can be chosen in the GUI. There are some manual operations, such as checking
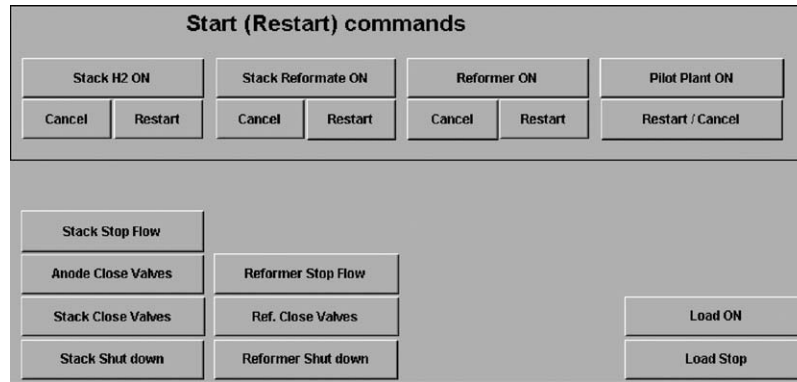
Fig. 5. Part of the graphical user interface (GUI) where all the start and stop buttons are shown.

that the manual valves are in correct position, that have to be confirmed by the operator before continuing the sequences. In the GUI, Fig. 5, the different stop buttons can be seen. There are different levels of shutting down and also possibilities to restart with the Restart buttons without having to start the complete sequence all-over again. If one in the middle is pressed, all above are included. One button, complete shutdown, shuts down the whole system. At the end of the stack and the fuel processor sequence, the components are purged with nitrogen again.

The fuel processor was delivered with a separate control system, which was supposed to be a slave during communication with the master control system. Unfortunately, the Modbus communication failed and the desired load level has to be written manually at the computer interface. Furthermore, the operator has to confirm that the fuel processor has been started. Therefore, the control strategy for the full system could not be fully automatic. To choose the load level, the natural gas flow to the fuel processor is set. The water and air intakes are thereafter controlled as a function of the natural gas intake and the internal temperature levels.

2.6.3. Surveillance

Several surveillance functions are included in the control system. The warning signals are divided into three attention levels; activation of any warning at the highest level results in a sound signal. The situations that lead to shutdown can be seen in Table 1.

If the ventilation fails, there are many devices that may ignite a hydrogen leakage, why a warning signal from the H_2 sensor

is used together with the ventilation failure signal to cut the electricity to the room. Furthermore, it was decided that the system always should be operated by personnel. The operators also have portable personal alarms for detection of small local CO leaks.

3. Results

3.1. The integration of the fuel processor

For the investigation of the integration of the fuel processor in the fuel cell system, its performance has been experimentally and theoretically analysed.

3.1.1. Start-up

Typical start behaviour of the fuel processor is displayed in the Fig. 6. The fuel processor is heated by combustion of natural gas. It takes approximately 4 min to reach an operating temperature close to 900 °C in the combustor. The temperature rise in the ATR reactor is based on the heat from combustion, and the start of the natural gas process flow. The air flow is not started until 20 min later. During the first two hours there are large amounts of carbon monoxide in the product gas and the methane slip is rather high, Fig. 6a. The CO level falls below the 10 ppm limit 2 h and 5 min after the fuel processor was started, but as seen in Fig. 6b the temperatures of the LTS and PROX reactors do not reach steady state until after 4 h and 30 min.

At steady state the gas composition has been evaluated to $48.4 \pm 0.4\%$ H_2, $17.1 \pm 0.3\%$ CO_2, $3.4 \pm 0.2\%$ CH_4 and 2.8 ± 0.4 ppm CO, cf. the 15 last minutes shown in Fig. 6a. The

Table 1
The situations causing actions by the control system

| Situation	Action
High CO or H_2 level in the room	Complete shutdown of the system
Ventilation off for a given length of time	Complete shutdown of the system
The CO level in the reformate is too high for the stack	Shutdown of the load and interruption of the flows to the stack as well as purging the stack with nitrogen
The temperature of the reformate is too high for a given length of time	Shutdown of the load and interruption of the flows to the stack
The pressure difference between the anode and the cathode is too high	Shutdown of the load and interruption of the flows to the stack
One of the cell voltages is lower than a predefined value for a given length of time	Shutdown of the load
The stack voltage is lower than a predefined value for a given length of time	Shutdown of the load
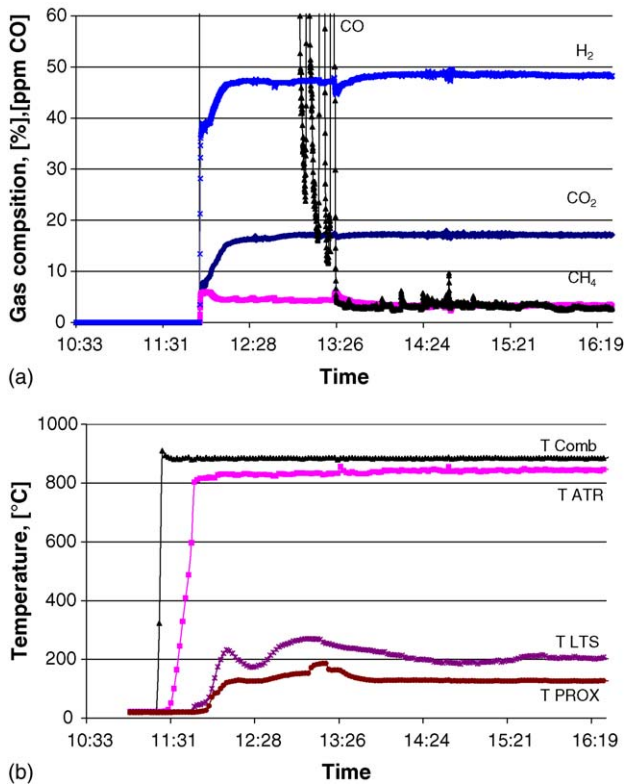
Fig. 6. (a) The gas composition of the reformate during start-up. The process fuel flow was started at 11.43. (b) Temperature levels of the combustion and the three reactors in the fuel processor.

CO level is well below its limit as given by the manufacturer, but the CH$_4$ level is higher than given by the manufacturer.

3.1.2. Load change

Table 2 shows gas compositions before and after a load change. It takes 12 min, Fig. 7, from 17.48 to 18.00, to change from 22.7 to 10.9 Nl NG min^{-1} (process NG), mainly depending on the time limits in the control strategy. The CO level is sufficiently low, below 10 ppm, but the methane level higher than expected after the load change. The maximum CO level due to the load change is 9.5 ppm.

A possible reason for the CH$_4$ level being lower during the load change, see Fig. 7a, is that the decrease in air flow is slower than the decrease in methane flow, giving a higher O/F ratio, Fig. 7b, and a better CH$_4$ utilisation. The change in water flow is even slower, as illustrated by the S/C ratio in the
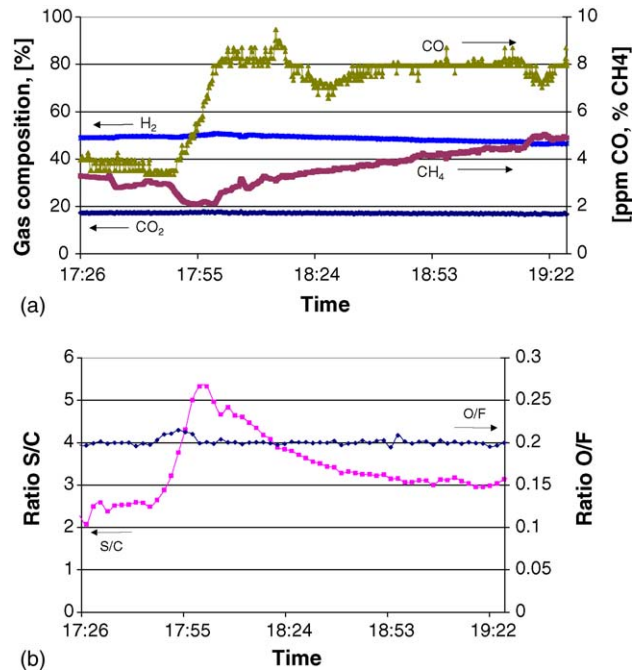

Fig. 7. (a) Gas composition of the reformate during a load change. After the load change the steady state is disturbed, which in this case has caused the CH$_4$ level to exceed 5%. (b) Stoichiometric steam to carbon ratio, S/C, and oxygen to fuel ratio, O/F, during the load change.

same figure. All oxygen fed to the ATR is really being used for the CPO reactions. Excess water, however, does not affect the reactions much, since the amount is already well above the stoichiometric ratio. The reason for limiting the oxygen to fuel ratio is both an increased hydrogen production by the steam reforming, and the risk of coking when the oxygen to fuel ratio exceeds 2.2.

The lower load level was shown to give a lower efficiency of the fuel processor. To start with, the constant natural gas flow to the combustor is relatively high, causing a lower efficiency and warmer exhausts, although the ATR temperature is lower than for the higher load level. Furthermore, the water flow is rather high—the control strategy is not tuned to provide the required low flow. Fig. 7a shows how the methane balance is disturbed, although a new steady-state is not awaited.

3.1.3. The dynamic behaviour

The slow dynamic behaviour, both during start-up and during load change, of the fuel processor is easily explained by the fact of its control strategy and parameters not being optimised. The input parameter for each controlled flow, such as each part of the distribution of the water stream, is limited to a temperature measurement at a single point. The control strategies of a commercial system would naturally be more sophisticated.

3.1.4. Mass and energy balance

Gas compositions, mass flows, efficiencies, and heat losses for the fuel processor have been evaluated with the help of a steady state fuel processor model. The model is based on the following assumptions [36]:

Table 2
Gas composition of the reformate before and after the load change

	High load level	Low load level
Natural gas[a] (Nl min^{-1})	22.7	10.9
H$_2$ (%)	49.5	50.6
CH$_4$ (%)	3.0	2.6
CO (ppm)	3.4	8.2
CO$_2$ (%)	17.3	17.5
N$_2$[b] (%)	30.1	29.3

[a] Natural gas flow to the ATR.
[b] Balance (calculated).

- Ideal gases, polynomials for water–steam [37].
- Chemical equilibrium at the ATR reactor outlet temperature. Chemical equilibrium at the LTS reactor outlet temperature. The PROX reactor has a typical CO selectivity of 40%, and the assumed output level is 6 ppm. This in turn gives the air flow to the PROX reactor.
- Higher hydrocarbons react completely in the ATR reactor; they are assumed to react with oxygen in a partial oxidation reaction.
- Methane is treated as inert in the LTS and PROX reactors.
- Sulphur is supposed to be totally removed.
- A composition of natural gas from Denmark is used, in mol%: 1.32 CO_2, 0.33 N_2, 87.71 CH_4, 6.62 C_2H_6, 2.86 C_3H_8, 1.16 C_4H_{10} and higher hydrocarbons [38]. (The gas contains <12 ppm sulphur of which <5 ppm is natural and the rest is added of detection reasons.)
- No heat losses are included, and pressure drops are neglected; 1.2 bar(a) is the assumed system pressure.

To use the model for estimation of the performance of the real equipment the measured methane slip through the fuel processor is added. The data input to the model is based on temperatures measured in the reformer and the gas compositions presented in Fig. 6.

The measured gas composition presented above for the higher load level is compared to the calculated values from the model, Table 3. The comparison indicates only a small mismatch in nitrogen content. Nitrogen, i.e. air, is added at two points in the fuel processor, both to the ATR reactor, and directly to the PROX reactor. As seen in Table 4, the air flow to the PROX reactor is only 2% of the total air flow. The total amount of air could be multiplied by a factor 1.04 to give the modelled hydrogen and nitrogen contents an exact fit with those measured; this factor is clearly negligible.

The measured data, in combination with the modelling work, gives a complete picture of the flows in and out from the fuel processor for the higher load level, Table 4. Neither fuel nor air flow to the combustor is measured, thus only the exhaust composition may give an assumption of these flows, and thereby the total amount of natural gas spent per unit reformate produced. The

Table 3
Measured (dry) gas composition of the reformate at steady state, and calculated composition at the high load level

	Measured	Calculated
H_2 (mol%)	48.4	49.3
CO_2 (mol%)	17.1	17.3
CO (ppm)	3	6
O_2 (mol%)	0.0	0.0
N_2 (mol%)	30.7[a]	29.7
CH_4 (mol%)	3.4	3.4
C_2H_6	–	–
C_4H_8	–	–
C_6H_{10}	–	–
Ar (mol%)	0.4[a]	0.3
Volume flow (Nl min^{-1})(g)	N.A.	128
Water content in flow (l min^{-1})(l)	N.A.	0.025

[a] Balance (calculated).

Table 4
Resumé of the measured and calculated gas and water flows at the high load level

	Measured		Calculated (Nl min^{-1})(g)
	(Nl min^{-1})(g)	(l/min)(l)	
Natural gas to ATR	22.7		
Air to ATR	45.7		
Water to ATR		0.0758	
Exhaust gas, MF30	245		
Natural gas to the combustor[a]			6.4
Air to the combustor[a]			251
Air to PROX[b]			1.1
Total natural gas, MFC23	27.4		

[a] Calculated from exhaust gas composition.
[b] Based on 40% CO selectivity in PROX.

actual, extremely high, ratio of air into the combustor is worth noting, a solution acceptable only in prototype equipment, but not in a commercial product. The ratio is due to the chosen, simple, control strategy, which keep the fuel flow to the combustor constant, while the combustor temperature is controlled only by changing the air flow.

From Table 4 it is clear that the external measurement of the total natural gas flow slightly deviates from the sum of the internal measured natural gas flow and the calculated flow to the combustor. The deviation concerns 6% of the total amount of natural gas, and the larger flow was used in the calculations. Furthermore, the factors S/C and O/F differ from the values from the fuel processor and the calculation in the developed model. The deviation in O/F is approximately 10%, and in S/C approximately 20%; both depend on the assumed composition of the natural gas. Fig. 7 shows the values. However, all the deviations described above are negligibly small. Hence, the results of the mass and energy balance can be utilised in further calculations.

The calculated intermediate gas compositions between the reactors in the fuel processor are illustrated in Fig. 8. The figure reflects the model assumptions presented above.
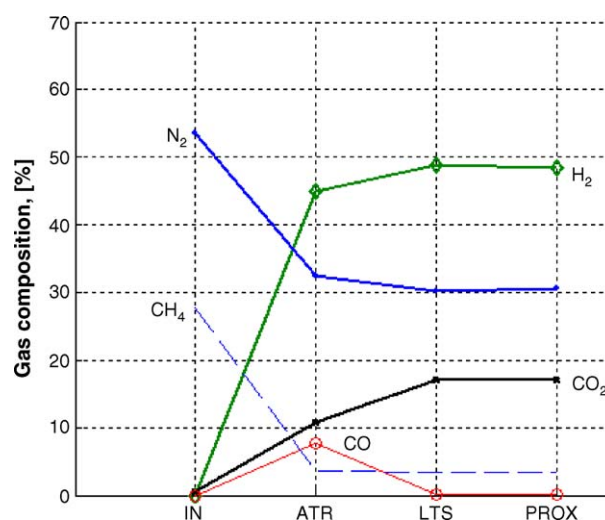

Fig. 8. Calculated ideal (dry) gas composition at steady state with actual pre-requisites (incl. CH_4 slip), at the ATR inlet, ATR outlet, LTS outlet, and PROX outlet.
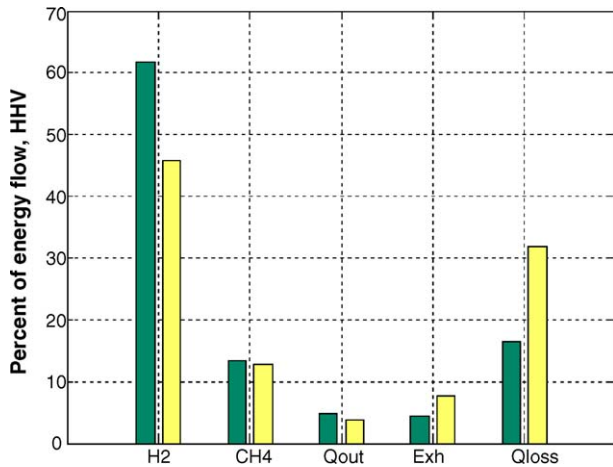
Fig. 9. Energy balance for the fuel processor at the two load levels, the higher level to the left. H_2: hydrogen in reformate CH_4: methane in reformate Qout: heat in reformate, down to $25\,^{\circ}C$ Exh: heat in combustion exhaust Qloss: the heat loss inside the fuel processor.

The achieved efficiency of the fuel processor at the higher load level is 62%, based on the HHV for hydrogen in the reformate, and total natural gas amount. The CH_4 slip stands for more than 13%, while the heat losses are approximately 16%, Fig. 9. The efficiency for the lower load level is as low as 46%. Furthermore approximately 300 W auxiliary electrical power is needed for air compressor and control system, according to the supplier.

3.1.5. Measurement equipment

The main problems with the integration of the fuel processor within the system are connected to its measurement equipment. One problem is condensation of water in the reformate within the mass flow meters and humidity meters. Another problem is that the mass flow meter is calibrated for a specific dry gas composition, which however varies. Due to deviations in the actual composition compared to the calibrated composition, conversion factors are used to give the correct mass flow values. The dry gas gives a proper value for MF31 in the lower flow range, but due to installation space savings (straight pipes of altogeher approximately 1 m would have been required before and after the mass flow meter) the reading becomes more incorrect for larger flows, up to 10% deviation. Additionally, humid flow gives even larger values.

3.2. The integration of the fuel cell stack

To date, the fuel cell stack has been integrated with the inverter and load system as well as the hydrogen and air supply systems. The stack performance degraded substantially already after a short time of operation, which prevented the planned evaluation of the integration of the fuel cell stack and the fuel processor.

During an exemplifying start-up (when using hydrogen), current and voltage levels were measured and summarised in a performance curve presented in Fig. 10. The performance verifies our utilisation of a previously developed semi-empirical
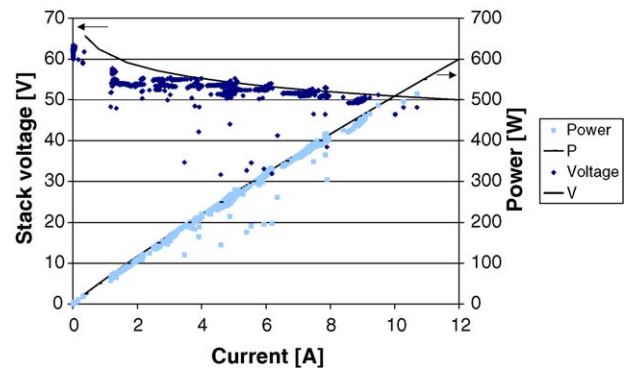

Fig. 10. The polarisation curve and the power level as functions of current for the fuel cell stack, data collected during three hours of operation. The lines P and V represent the calculated power and voltage levels.

fuel cell model [39–41]. Within the operated temperature and pressure ranges the model gives hardly any variations. It is further quite natural that the fuel cell stack – not operating at steady state – shows worse results than the model, which does not include dynamics, water condensation or start-up. The fuel cell stack is started by gradually increasing the load signal, Fig. 11b. The stack temperature rises as the stack produces power, Fig. 11a. During operation of the stack, the input flows are regulated to be large enough to avoid condensation of water.

It takes several minutes to reach steady state for a wanted load level, Fig. 11b. Even for a load connected to the fuel cell
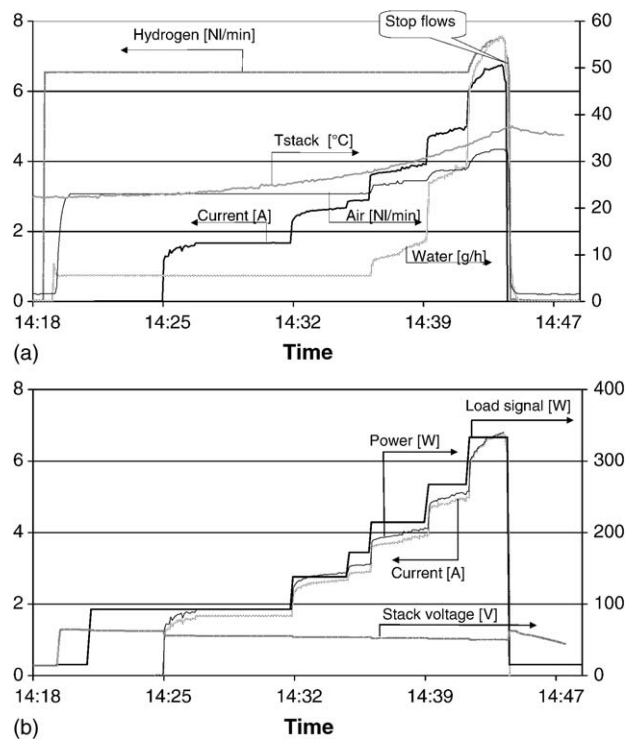

Fig. 11. (a) Temperature increase and current-following flows of hydrogen, water and air during start-up. (b) The load characteristics at start-up. As described the load signal is the signal from the control system to the power regulator, here scaled down.
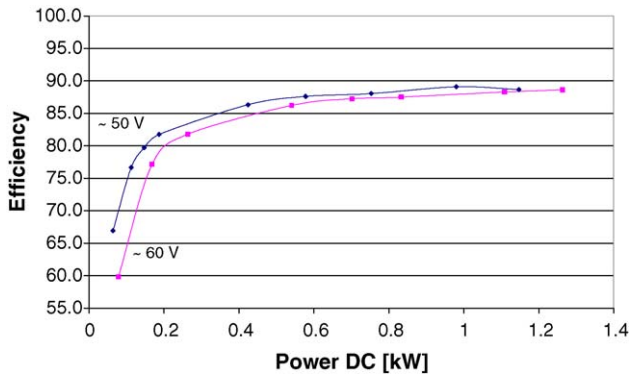
Fig. 12. The efficiency of the inverter, as function of load level and input voltage, 50.5–46.8 V and constant at 60.1 V, respectively.

stack without the inverter it takes several minutes to reach steady state.

The cell voltages in the stack have shown to be unstable. Especially some cells are sensitive giving a decrease in cell voltage as a usual result during operation. The presented fuel cell stack data is from the initial experiments, and later experiments have shown a significant degradation. Another observation is that automatic pressure-reducing valves are desirable after the anode and cathode for better control of the pressure in the fuel cell stack.

3.2.1. Mass flow controllers

The mass flow controllers providing gas to the stack all have time delays. The hydrogen mass flow controller (MFC12) responds within 5 s, while the humidification water mass flow controller (MFC15) takes about 40 s to respond, and the air mass flow controller (MFC13) takes even 10 more seconds before it starts to increase towards the desired air flow, which in turn is reached after a further 40 s. It is important to be aware of the time delays of the mass flow meters, not to add a load to the fuel cell stack before additional air has been provided.

3.2.2. CO sensors and safety regulation

The CO sensors have been proven to detect carbon monoxide, but also hydrogen. A few times during operation of only the fuel cell stack, small flows of hydrogen-rich gas were released into the room, and for this reason the automatic shut down of the system at CO indication had to be aborted.

3.3. The integration of the inverter and the load system

For evaluation of the inverter and the load system, without disturbances from the fuel cell stack, a separate power supply was connected to the inverter. As can be seen from Fig. 12 the efficiency of the inverter depends on the input voltage. Furthermore, the voltage history affects the present power level. This fact implies that a fixed requested load level from the control system in reality will make the power level vary as a function of the previous stack voltage.

4. Discussion

Although experiments on the fuel cell system gives specific results for the components in the system, the main objective of this paper has been to study the interaction of the components. The results show that it is difficult to integrate components into a system, if they are not matched already at the design phase. Furthermore, the measurement equipment installed for research purposes will affect the system performance. As presented above, the mismatch in size of the fuel processor and the fuel cell stack has implied in special solutions in the system configuration, thus the fuel cell system studied in the test facility cannot be directly compared to a commercial system. To start with, the mismatch prevents feedback of the anode off-gas to the fuel processor. Instead, natural gas is combusted in order to maintain the temperature of the fuel processor, resulting in a lower efficiency of the system. Further, there is a lack of equipment such as air compressor and heat measuring devices. The heat produced in the fuel cell, which could have been transferred to a hot-water storage, is released into the surroundings whereby the heat balance cannot be directly studied. Although the components are spread out in the laboratory the temperatures of the gas flows are maintained with the help of heating cables compensating for heat losses to the surrounding.

Two of the main objectives of the control system were to have surveillance and automatic operation of the system. This has also been achieved, but at the expense of simplicity when running parts of the system. The presented division of the control system into modes and sequences simplifies the operation and surveillance. The main inconvenience occurs when operating the system manually and when the conditions for non-automatic equipment must be confirmed. The sequences in the control system have been evaluated to be more extensive than needed. The automated routines will be more useful later in the project when the initial problems regarding the equipment have been solved. The programming of the sequences was made before the different components were tested and before the data logging function was programmed. When looking back, it would have been more straightforward and less time-consuming to first build up the logging system, and then build up and test each part of the system separately. Thereafter the sequences should have been designed, and the system integrated. The control system software chosen is more suited for a plant whose operational conditions are well known. The log system has been evaluated to be stable, with a sufficient capacity in number of variables and time steps. The four running modes and the surveillance functions have on the other hand been shown to be well identified, and of importance for the experimental purposes. Finally, the fact that the separate control system for the fuel processor does not have any contact with the main control system causes complete automation of the system to be impossible. It does not, however, affect the planned experiments.

However, although the test facility cannot be considered as optimal it does support experiments in future research on fuel cell systems, and the concept of having well spread-out components in the laboratory has simplified both re-building and demonstrations.

5. Conclusions

The characteristics of all the components chosen for a specific fuel cell system strongly affect the quality of the integration and thereby the system performance. The main limitation in the system configuration presented in this paper is the size mismatch of the fuel cell stack and the fuel processor due to the poor availability of components at the time of purchase. Another limitation is the problems with some measurement equipment, which would enable a complete analysis of mass and energy flows in the whole system. However, the research PEFC test facility has a simple and flexible configuration, with extensive measurement equipment and a rigorous control system.

- The fuel processor gives a stable hydrogen content (approximately 50%) in the reformate gas, but a higher methane content (approximately 3%) than given by the manufacturer. The response time for a load change of the fuel processor is approximately 10 min. The efficiency of the fuel processor, at a load level corresponding to $4\,kW_{el}$, is estimated to 62% (HHV), and the internal losses are identified, also at a partial load level. The CO content in the reformate is low (below 10 ppm).
- The time it takes to increase the gas flows to the fuel cell stack is a limiting factor when a higher power level is requested. Additionally, the PEFC stack has shown a quite limited power output, and unstable operation, which has been getting worse with time.
- The inverter in connection to the power regulator has shown a non-constant power output at required load level. Furthermore, the efficiency of the inverter depends on the input voltage.

6. Future work

The research PEFC system serves as a good platform and basis for future research and development on small-scale stationary PEFC systems.

An on-going re-building of the system is connected to the replacement of the old fuel cell stack by a new, larger one. Thereafter, the goal is to integrate the fuel cell stack with the fuel processor, which includes studies of the stack performance when run on reformate.

Dynamic simulation models of the components will be developed and verified with experimental data to aid the analysis of for example the control strategies for a PEFC system. This work includes further experiments on the parameter impact on the efficiencies and gas composition of the fuel processor. The study will include partial loads.

Appendix A

Symbol	Equipment	Measuring range	Manufacturer	Type	Type of signals
⊏F⊐ MFC10	Mass flow controller	$2–100\,Nl\,min^{-1}$ (38% H_2, 13% CO_2, 49% N_2), $T = 65\,°C$	Bronkhorst Hi-Tec	F-103D-FGB-55-V/ F-004BC valve	AO, AI
MFC11	Mass flow controller	$1–50\,Nl\,min^{-1}$ H_2	Bronkhorst Hi-Tec	F-201AC-FGB-22-V	AO, AI
MFC12	Mass flow controller	$0.2–10\,Nl\,min^{-1}$ H_2	Bronkhorst Hi-Tec	F-201C-FDC-22-V	AO, AI
MFC13	Mass flow controller	$0–600\,Nl\,min^{-1}$ air	Bronkhorst Hi-Tec	F-203AC-FGB-55-V	AO, AI
MFC15	Mass flow controller	$2–100\,g\,h^{-1}$ distilled H_2O	Bronkhorst Hi-Tec	L1-FDC-22-0	AO, AI
MF21	Mass flow meter	$2.1–105\,Nl\,min^{-1}$ N_2, $T = 65\,°C$	Bronkhorst Hi-Tec	F-103D-HGD-55-V	AI
MF22	Mass flow meter	$12–600\,Nl\,min^{-1}$ air, $T = 70\,°C$	Bronkhorst Hi-Tec	F-106ZI-HGD-02-V	AI
MFC23	Mass flow controller	$2–100\,Nl\,min^{-1}$ (38% H_2, 13% CO_2, 49% N_2), $T = 65\,°C$	Bronkhorst Hi-Tec	F-103D-FGB-55-V/F-004BC valve	AO, AI
MF30	Mass flow meter	$2–40\,Nm^3\,h^{-1}$, $T = 200–250\,°C$	Bronkhorst Hi-Tec	EMO Turbine meter, GLFL1	AI

Symbol	Equipment	Measuring range	Manufacturer	Type	Type of signals
MF31	Mass flow meter	4–200 Nl min^{-1} 38% H_2, 13% CO_2, 49% N_2, $T = 65\,°C$	Bronkhorst Hi-Tec	F-106ZI-HGD-02-V	AI
(pressure symbol)	Pressure meters	0–200 mbar	Valcom	86F-P-01	AI
(thermocouple symbol)	Thermocouples	Type K	Eurotherm	type K	
(thermocouple symbol) T15	Thermocouple	Type T	Eurotherm	type T	
(A symbol)	Current measurement	0–30 A	ABB		AI
(V symbol)	Voltage measurement		ABB		AI
(% symbol)	Humidity sensors	0–100% RH, 50–150 °C	Panametrics	MCHTR-1	AI
(valve symbol)	Control valves	On/off (1/0 or 0/1)	Bürkert	5282	DO
CO sensor		0–500 ppm	BW Technologies		AI
H_2 sensor		0–100% LEL	BW Technologies		AI
FCV01, etc.	Single cell voltages	0–1 V			AI
P1	Pump	On/off	March	MDXT	DO
HEX1	Heat exchanger with fan	On/off	Comair Rotron (fans)		DO
C20	Contactor	On/off	ABB	ESB 40-40	DO
C21	Contactor	On/off	ABB	ESB 24-40	DO
EV11	Evaporator for hydrogen stream	0–200 °C	Bronkhorst Hi-Tec	CEM, W-202-NNO-P, 100 W	AI
Gas analysis system			ABB Analytical	Advance Optima	
	Hydrogen	15–0%/75–0%		V24721A, Caldos 17	AI
	Carbon monoxide	0–50 ppm/0–500 ppm		V24511A, Uras 14	AI
	Carbon dioxide	0–10%/0–40%		V24721A, Caldos 17	AI
	Hydrocarbons	0–3%/0–6%		V24721A, Caldos 17	AI
	Oxygen	0–25% in N_2, 0–10%/0–15%/0–25%, 0–100% in the other gases		V24611A, Magnos 16	AI
Further equipment					
Stack	Fuel cell stack	0–2 000 W_{el}			
Reformer	Fuel processor with CO clean-up[a]	0–10 000 W_{el}			
Inverter	dc/ac inverter	44–60 VDC/220–240 VAC, 3300 VA	Trace Engineering	SW3048E	
Load	Electric load (AC)	0–2 000 W_{el}	ConVector 2000	Regent, convector radiator HC2000	
CT1	Expansion tank		Amtrol	model No 15	
W01	Pressurised water container				
GA	Heated sample gas line		ABB Analytical	CGWB13	
Heating cables		39 W m^{-1} @10 °C	Raychem Chemelex Auto-trace	12XTV2-CT	
Regulators		40–95 °C, regulating tolerance 1–10 °C	Termonic	16150	
Insulation			Armaflex	Thickness 19 mm, Ø 44 mm	
Cool1	Cooling medium, stack	Boiling temperature, 60 °C	3M	NovecTM Engineered fluid, HFE-7100	
Cool2	Cooling medium, reformer			Tap water	
Tubes	Stainless steel			SS2333	
Tubes	Plastics			PFA	
Fittings	Stainless steel		Swagelok		
(valve symbol)	Needle valve		Swagelok	SS-1RS8	
(drain symbol)	Drain		Swagelok	Manual valves	
Air supply system					
L1	Micro filter	0.8 m^3 min^{-1}	Biab tryckluft	Filter model G3XP. Filter element 1050 XP	
L2	Oil vapour adsorber	8501 min^{-1}	Zander	AK575	
Air humidifier			ABB	Own design, not commercial	

Symbol	Equipment	Measuring range	Manufacturer	Type	Type of signals
EL1	Immersion heater	3 kW	Energi Ekonomi	6210272, stainless steel 316L	
VR1	Safety relief valve		IMI Bailey Birkett Ltd.	706 Series	
B3	Catalytic burner				
	Catalyst		OMG Automotive catalyst		
	Catalyst house		Ferrita Sweden AB		

[a] The CPO and SR catalysts consist of noble metals on a ceria base. The desulphurisation unit has a ZnO catalyst, while the catalyst in the LTS reactor is from Süd Chemie. The PROX reactors contain a catalyst from Engelhard.

References

[1] S. Lux, M. Binder, F. Holcomb, N. Josefik, The DoD residential PEM fuel cell demonstration program, Fuel Cell Bull. (2003).

[2] S. Geiger, M. Cropper, Fuel cell market survey: small stationary applications, Fuel Cell Today (2003), www.fuelcelltoday.com, accessed 1 November 2003.

[3] M. Cropper, S. Geiger, D. Jollie, Fuel Cell Systems: a survey of worldwide activity, 5 November 2003. www.fuelcelltoday.com, accessed 1 December 2003.

[4] G. Gigliucci, L. Petruzzi, E. Cerelli, A. Garzisi, A. La Mendola, Demonstration of a residential CHP system based on PEM fuel cells, J Power Sources 131 (2004) 62–68.

[5] T. Mizukami, T. Okusawa, K. Takahashi, N. Imada, Y. Enokizu, 1 kW class PEFC system using internal heating fuel processor—fine transient responsibility for residential electricity demands, in: Proceedings of the 2003 Fuel Cell Seminar, 3–7 November 2003, Miami Beach, USA, 2003.

[6] H. Ohara, Y. Yamanaka, M. Mizusawa, A. Suzuki, K. Kobayashi, Development of 5 kW PEFC system, in: Proceedings of the 2003 Fuel Cell Seminar, 3–7 November 2003, Miami Beach, USA, 2003.

[7] C. Wunderlich, F. Reichenbach, PEM Fuel Cell Cogeneration power plant optimisation—on the way to a commercial product, Offset- und Dissertations-Druck Kinzel, Göttingen, Germany, in: Proceedings of the international conference with exhibition, The Fuel Cell Home, 2–6 July 2001, Lucerne, Switzerland, 2001, ISBN 3-905592-07-X, pp. 133–142.

[8] K. Shindo, T. Ouki, O. Tajima, N. Nishizawa, T. Susai, Development of a PEFC co-generation system for residental use, in: Proceedings of the 2000 Fuel Cell Seminar, pp. 492–495, 30 October–2 November, Portland, USA, 2000, pp. 260–262.

[9] X. Francois, M.-C. Péra, D. Hissel, J.-M. Kauffmann, Design of a test bench for low power PEMFC, Offset- und Dissertations-Druck Kinzel, Göttingen, Germany, in: Proceedings of the international conference with exhibition, 1st European PEFC Forum, 2–6 July 2001, Lucerne, Switzerland, 2001, ISBN 3-905592-08-8, pp. 491–499.

[10] V. Naso, M. Lucentini, M. Aresti, Evaluation of the overall efficiency of a low pressure proton exchange membrane fuel cell power unit, American Institute of Aeronautics and Astronautics, Inc., AIAA-2000-2003, 2000, pp. 1147–1150.

[11] G. Heideck, M. Purmann, Z. Styczynski, Micro-computer control for a fuel cell text bench for residential use, J. Power sources 127 (2004) 319–324.

[12] College of the Desert and SunLine Transit Agency, Hydrogen fuel cell engines and related technologies, course manual, Revision 0, December 2001. http://www.eere.energy.gov/hydrogenandfuelcells/fuelcells/h2_manual.html, accessed 1 November 2002.

[13] Y. Nakamoto, N. Kato, T. Hasegawa, T. Aoki, S. Muroyama, 4.5-kW fuel cell system based on PEFCsdkjdot, in: Proceedings of the 22nd International Telecommunications Energy Conference (INTELEC 2000), 10–14 September 2000, Phoenix, AZ, USA, 2000, pp. 406–410, Institute of Electrical and Electronics Engineers Inc.

[14] Z. Barisic, European field trial program with 250 kW PEM fuel cell power plants, in: Proceedings of the international conference with exhibition, The Fuel Cell Home, 2–6 July 2001, Lucerne, Switzerland, Offset- und Dissertations-Druck Kinzel, Göttingen, Germany, ISBN 3-905592-07-X, 2001, pp. 187–196.

[15] E. Torrero, R. McClelland, Residential Fuel Cell Demonstration Handbook, NREL/SR-560-32455, Subcontract No. AAD-1-30605-12, NREL National Renewable Energy Laboratory, Contract No. DE-AC36-99-GO10337, July 2002.

[16] D.J. Edlund, W.A. Pledger, A. Dickman, Field testing residential fuel cell systems, in: Proceedings of the 2000 Fuel Cell Seminar, Portland, USA, 2000, pp. 496–498.

[17] H.I. Lee, C.H. Lee, T.Y. Oh, S.G. Choi, I.W. Park, K.K. Baek, Development of 1 kW class polymer electrolyte membrane fuel cell power generation system, J. Power Sources 107 (2002) 110–119.

[18] H.S. Lee, K.S. Jeong, B.S. Oh, An experimental study of controlling strategies and drive forces for hydrogen fuel cell hybrid vehicles, Int. J. Hydrogen Energy 28 (2003) 215–222.

[19] B.K. Datta, G. Velayutham, A.P. Goud, Fuel cell power source for a cold region, J. Power Sources 106 (2002) 370–376.

[20] Z. Styczynski, M. Purmann, E. Handschin, S. Malcher, J. Scholta, L. Jörissen, University fuel-cell-laboratory for research and teaching purposes, concept, planning and operation experiences, Offset- und Dissertations-Druck Kinzel, Göttingen, Germany, in: Proceedings of the international conference with exhibition, 1st European PEFC Forum, 2–6 July 2001, Lucerne, Switzerland, 2001, ISBN 3-905592-08-8, pp. 501–511.

[21] J. Hamelin, K. Agbossou, A. Laperrière, F. Laurencelle, T.K. Bose, Dynamic behavior of a PEM fuel cell stack for stationary applications, Int. J. Hydrogen Energy 26 (2001) 625–629.

[22] F. Harel, D. Hissel, M.C. Péra, First experimental results on a 5 kW PEMFC testing bench linked to constraints of the transportation systems, Offset- und Dissertations-Druck Kinzel, Göttingen, Germany, in: Proceedings of the international conference with exhibition, the 2nd European PEFC Forum, vol. 2, 30 June–4 July 2003, Lucerne, Switzerland, 2003, ISBN 3-905592-13-4, pp. 507–516.

[23] J.C. Cross III, W.L. Mitchell, P. Chinatawar, M. Hagan, C. Thompson, D. Swavely, PEM fuel cell power system technology, in: Proceedings of the Fuel Cell Seminar, 30 October–2 November, 2000, Portland, USA, 2000, pp. 260–262.

[24] F. Harel, S. Jameï, X. François, M.C. Péra, D. Hissel, J.M. Kauffmann, Experimental investigations on PEMFC: a test bench design, in: Proceedings of the France Deutschland Fuel Cell Conference, 7–10 October 2002, Forbach, 2002.

[25] ZSW ECW Systemtechnik von Brennstoffzellenanlagen, www.zsw.uni-ulm.de/ecw/systech/overview.htm, accessed 21 December 2000.

[26] J. Mathiak, A. Heinzel, J. Roes, Th. Khalk, H. Kraus, H. Brandt, Coupling of a 2.5 kW steam reformer with a 1 kW$_{el}$ PEM fuel cell, J. Power Sources 131 (2004) 112–119.

[27] M.B.V. Virji, P.L. Adcock, P.J. Mitchell, G. Cooley, Effect of operating pressure on the system efficiency of methane-fuelled solid polymer fuel cell power source, J. Power Sources 71 (1998) 337–347.

[28] N.S. Arvindan, B. Rajesh, M. Madhivanen, R. Pattabiraman, Hydrogen generation from natural gas and methanol for use in electrochemical energy conversion systems (fuel cell), Indian J. Eng. Mater. Sci. 6 (1999) 73–86.

[29] S. Ahmed, J. Kopasz, R. Kumar, M. Krumpelt, Water balance in a polymer electrolyte fuel cell system, J. Power Sources 112 (2002) 519–530.

[30] B. Vogel, G. Schaumberg, A. Schuler, A. Heinzel, Hydrogen generation technologies for PEM fuel cells, No. 1100, in: Proceedings of the Fuel Cell Seminar, 16-19 November 1998, Palm Springs, USA, 1998.

[31] V. Recupero, L. Pino, R. Di Leonardo, M. Lagana, G. Maggio, Hydrogen generator, via catalytic partial oxidation of methane for fuel cells, J. Power Sources 71 (1998) 208–214.

[32] M. de Francesco, E. Arato, Start-up analysis for automotive PEM fuel cell systems, J. Power Sources 108 (2002) 41–52.

[33] J.M. Zalc, D.G. Löffler, Fuel processing for PEM fuel cells: transport and kinetic issues of system design, J. Power Sources 111 (2002) 58–64.

[34] J.M. Ogden, Review of small stationary reformers for hydrogen production, Report to the International Energy Agency, Technical contact Elam, C. at NREL, 9 March 2001.

[35] Lewis, R. W., Programming industrial control systems using IEC 1131-3, London: Institution of Electrical Engineers, ISBN 0-85296-950-3, 1998.

[36] C. Wallmark, P. Alvfors, Design of stationary PEFC system configurations to meet heat and power demands, J. Power Sources 106 (2002) 83–92.

[37] L. Wester, Tabeller och diagram för energitekniska beräkningar, Mälardalens Högskola, Västerås, 1998 (in Swedish).

[38] Dong, www.dong.dk, January 2001. Accessed 27 February 2001.

[39] R.F. Mann, J.C. Amphlett, M.A.I. Hooper, H.M. Jensen, B.A. Peppley, P.R. Roberge, Development and application of a generalised steady-state electrochemical model for a PEM fuel cell, J. Power Sources 86 (2000) 173–180.

[40] J.C. Amphlett, R.M. Baumert, R.F. Mann, B.A. Peppley, P.R. Roberge, Performance modeling of the Ballard Mark IV solid polymer electrolyte fuel cell II, J. Electrochem. Soc. 142 (1) (1995) 9–15.

[41] J.C. Amphlett, R.F. Mann, B.A. Peppley, P.R. Roberge, A. Rodrigues, A practical PEM fuel cell model for simulating vehicle power sources, in: Proceedings of the 10th Annual Battery Conference on Applications and Advances, 10–13 January 1995, Long Beach, CA, USA, Publisher IEEE, New York, 1995, pp. 221–226.